Command Shaping Applied to Nonlinear Systems with Configuration-Dependent Resonance

Victor M. Beazel and Peter H. Meckl, *Member, IEEE*

***Abstract*—A primary obstacle to employing the standard command shaping approach to flexible nonlinear systems is the variation in resonant frequencies of these systems with changes in geometry. A modified shaping technique involving trajectory segmentation that extends the benefits of command shaping to these types of systems is presented.**

I. Introduction

DYNAMIC systems that are designed for rapid repositioning are typically pushed to the point where they exhibit flexible behavior that hinders the accomplishment of the purpose for which they were designed. Remedial techniques are frequently employed to either enable these systems to achieve the objectives of their original design, or to extend their operating envelope beyond the design limits that were initially envisioned by their designers.

Some techniques concentrate on increasing system damping, which may be active or passive in nature. Other techniques, such as command shaping, focus on selecting appropriate input commands to drive a system to its desired final position, without exciting the system's natural frequencies. Command shaping is the focus of this present work. While there has been much accomplished in this area for linear systems with fixed natural frequencies, investigation of appropriate ways to extend these methods to systems with configuration-dependent resonance is still in its infancy.

With this objective in mind, a gimbaled telescope turret has been modeled in such a way that it possesses a configuration-dependent resonant frequency. The standard command shaping approach has been applied to the system model, demonstrating that in some cases it produces more vibration than without shaping. The research described in this article has successfully extended the command shaping methodology to accommodate nonlinear systems with resonance that varies with changes in mechanical geometry, thereby providing significant reduction in endpoint vibration of the system response over that of the unshaped case.

Manuscript received September 27, 2004. This work was supported in part by the U.S. Air Force Research Lab, Kirtland AFB, NM.

V. M. Beazel is with the USAF Research Lab, Kirtland AFB, NM, 87117 USA; phone: 505-853-7037, fax: 505-853-6151, e-mail: Victor.Beazel@kirtland.af.mil

P. H. Meckl, is with the School of Mechanical Engineering, Purdue University, West Lafayette, IN, 47907 USA.

II. Command Shaping Approaches

The various command shaping approaches might be classified within one of three basic categories: (1) constrain system inputs to be band-limited, (2) convolve the inputs with a Finite Impulse Response filter, (3) synthesize the input commands using basis functions. The relative merits of this latter command shaping approach over those of the first two, for time-invariant linear systems, has been discussed by DeRoover and Sperling [1].

The application of command shaping to frequency-variant systems is still in its infancy. The work of Park and Chang [2] and of Park, Chang, and Lee [3], involving some type of repetitive learning scheme for tuning a nonlinear filter is typical of research efforts in this area. These approaches were applied primarily to simplistic models. The drawback with much of this work is that for many systems and/or applications, these repetitive learning schemes are infeasible. Book and Magee [4] have developed an innovative approach where the filter time delays have been made adaptive in nature, but it was found that in some cases, the time delays could take on unacceptably large values. All these efforts may be classified as being in Category 2.

One of the early attempts to apply the command shaping techniques of Category 3 to time varying systems, has been made by Kinceler and Meckl [5], in which shaped commands were synthesized using the finite-time Laplace transform with a segmented trajectory. Implementation issues were encountered and this research was never completed.

III. Synthesis of Command Functions

The method proposed by Meckl [6] for command shaping was to create a weighted, multi-objective cost function that minimizes the square of the difference between a synthesized command function profile of the form $f_{cs}(t) = \tau_m \sum_{k=1}^{L} \beta_k \Phi_k$, and a bang-bang or square-wave command function, while penalizing the magnitude of the Fourier transform in the spectral region of the natural frequencies of the system,

$$J_c = \underbrace{\frac{1}{T_f}\int_0^{T_f}\frac{1}{\tau_m^2}\left[f_r(t)-f_{cs}(t)\right]^2 dt}_{\text{Fit synthesized force profile to minimum time profile,}} + \underbrace{\rho\sum_{i=1}^{N}(\omega_i T_r)^2\left|F_{cs}^*(\omega_i T_f)\right|^2}_{\text{subject to attenuated spectral amplitude at modal frequencies.}} \quad (1)$$

where τ_m is the maximum torque available, β is a coefficient vector, Φ is a set of basis functions, T_r is the system move time corresponding to a square wave or bang-bang input, T_f is the move time associated with a command shaped input, f_r is the bang-bang force profile used to move a rigid-body system in a time-optimal manner, f_{cs} is the command shaped force, ω_i is the i^{th} natural frequency of the flexible system, ρ is the relative weighting between goodness of fit and the frequency domain penalty to be levied during the minimization process, and F_{cs}^* is the Fourier transform of the dimensionless command shaped force profile. The partial derivatives of this cost function with respect to the basis function coefficients of the shaped command are then set equal to zero, and the resulting linear system of algebraic equations can then be solved for the coefficients of the command profile.

IV. Model of Gimbaled Telescope

A gimbaled telescope turret is shown in Figure 1. It has an outer gimbal with two degrees of freedom, for the purpose of coarse-tracking a target of interest.

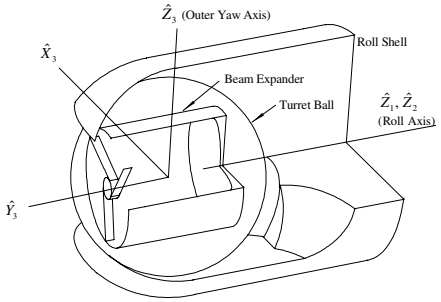

Fig. 1. Cutaway diagram of gimbaled telescope.

The first degree of freedom is defined as the roll shell motor position. The second degree of freedom is defined as the angular displacement due to the drive train compliance between the roll motor and the roll shell about the roll axis. This compliance separates the roll motor from the roll shell. The third degree of freedom involves a rotation of the turret ball, which houses the telescope beam expander, about an outer yaw axis, relative to the roll shell. There is also an inner gimbal with two additional degrees of freedom for the purpose of fine tracking. For the purpose of this study, however, the inner gimbal will be assumed to be caged, and is therefore not shown in Figure 1.

To accentuate the difficulties that configuration-dependent resonant frequencies pose to the standard command shaping approach, the imbalance in the inertial properties of the turret ball were made artificially large. The mass moment of inertia of the turret ball and its associated sub-assemblies, I_{3Y}, about $\hat{Y}_3$, is approximately two orders of magnitude greater than the inertia, I_{3X}, about $\hat{X}_3$, and approximately one order of magnitude larger than the inertia, I_{3Z}, about the yaw axis. As will be seen in Section 5.3.5, this exaggerated inertial imbalance gave rise to gyroscopic behavior that would tend to force the yaw angle, θ_3, toward zero for large roll axis velocities, like the torque that makes a spinning top stand up against the pull of gravity.

Using Craig's recursive formulation [7], the gimbaled telescope was described by a system of equations with the following form,

$$M_\theta \ddot{\theta} = \tau - V(\theta,\dot{\theta}) - U(\theta). \quad (2)$$

The roll shell was referenced to ground using the absolute coordinate $\theta_{12} = \theta_1 + \theta_2$, where θ_1 represents the roll motor position, and θ_2 represents the twist angle of the motor shaft connecting the motor to the roll shell. The resulting system is represented by,

$$\begin{bmatrix} m_{11} & 0 & 0 \\ 0 & m_{22} & m_{23} \\ 0 & m_{23} & m_{33} \end{bmatrix} \begin{bmatrix} \ddot{\theta}_1 \\ \ddot{\theta}_{12} \\ \ddot{\theta}_3 \end{bmatrix} = \begin{bmatrix} F_1 \\ F_2 \\ F_3 \end{bmatrix} \quad (3)$$

where

$m_{11} = I_{1Z}\, gr^2$, is the roll motor inertia scaled by the square of the gear ratio (gr = 718),

$$m_{22} = I_{2Z} + I_{3X} S_3^2 + I_{3Y} C_3^2 + m_2 (Y_{c2}^2 + X_{c2}^2) + m_3 (Y_{c3}^2 S_3^2 + Z_{c3}^2),$$

$$m_{23} = -m_3 Y_{c3} Z_{c3} C_3,$$

$$m_{33} = I_{3Z} + m_3 Y_{c3}^2,$$

$$F_1 = \tau_1 + K_2(\theta_{12} - \theta_1) + D_2(\dot{\theta}_{12} - \dot{\theta}_1),$$

$$F_2 = (m_2 X_{c2} + m_3 Z_{c3}) S_{12}\, g - m_3 \dot{\theta}_3^2 Y_{c3} Z_{c3} S_3 - 2\dot{\theta}_{12}\dot{\theta}_3 S_3 C_3 (I_{3X} - I_{3Y} + m_3 Y_{c3}^2) - (m_3 Y_{c3} S_3 - m_2 Y_{c2}) C_{12}\, g - K_2(\theta_{12} - \theta_1) - D_2(\dot{\theta}_{12} - \dot{\theta}_1),$$

$$F_3 = \tau_3 - m_3 Y_{c3} S_{12} C_3\, g + \dot{\theta}_3^2 S_3 C_3 (I_{3X} - I_{3Y} + m_3 Y_{c3}^2)$$

m_2 = mass of roll shell (5036 lbs.),
m_3 = mass of turret ball (5525 lbs.),
τ_1, τ_3 = applied torque about roll axis and yaw axis respectively,
K_2 = stiffness coefficient of roll motor drive shaft (1.1×10^{12} lbs-in/rad),
D_2 = damping coefficient of roll motor drive shaft (1.02×10^8),
$C_i = cos(\theta_i)$ and $S_i = sin(\theta_i)$,
X_{ci} = the offset from the center of the i^{th} reference to the i^{th} center of mass in the $\hat{X}_i$ direction (similar definitions apply to Y_{ci} and Z_{ci}),

X_{c2}= -0.3 in., Y_{c2}= 1.0 in., Y_{c3}= -0.2 in., and Z_{c3}= -0.5 in.

$I_{i\hat{u}}$ = mass moment of inertia about the $\hat{u}$-axis in the i^{th} reference frame.

I_{1z} = 6.4 lbs-in.-s^2, I_{2z} = 15.5x10^6 lbs-in.-s^2, I_{3x} = 7.5x10^5 lbs-in.-s^2, I_{3y} = 7.4x10^7 lbs-in.-s^2, and I_{3z} = 7.7x10^6 lbs-in.-s^2.

For this system with one decoupled equation, the acceleration vector, $\ddot{\theta}$, is easy to isolate without having to perform a matrix inversion. This step will simplify the numerical integration process. The final set of nonlinear equations describing the dynamics of the modified turret model is

$$\ddot{\theta}_1 = \frac{F_1}{m_{11}} \tag{4}$$

$$\ddot{\theta}_{12} = \frac{m_{23}F_3 - m_{33}F_2}{m_{23}^2 - m_{22}m_{33}} \tag{5}$$

$$\ddot{\theta}_3 = \frac{1}{m_{33}}\left[F_3 - m_{23}\frac{m_{23}F_3 - m_{33}F_2}{m_{23}^2 - m_{22}m_{33}}\right]. \tag{6}$$

V. Feedback Control of the Turret Model

Due to nonlinearities such as inertial imbalance of the turret ball, center of mass offsets, and gyroscopic behavior resulting from high velocity slew maneuvers, it was necessary to incorporate feedback control into the turret model. The approach employed was the computed torque method in conjunction with gain scheduling of the variable θ_3, to account for the main contribution to the system nonlinearity and to accommodate reference model uncertainties. The yaw angle, θ_3, is the parameter that drives the variability of the system resonant frequency. Details of this approach are given in [8]. Figure 2 shows the overall structure of the computed torque control law. The block labeled *N.L.* represents the nonlinear model of the turret. The variables with ^ shown in Figure 2 are approximations to their counterparts in (2). Note that the inertia matrix, $\hat{M}_\theta$, used to compute the torque inputs to *N.L.* was intentionally corrupted with between 5-10 % uncertainty, where the uncertainty values were arbitrarily selected. I_m is a unit inertia which serves to convert the servo-torque, τ', to acceleration units. The variables, k_v and k_p, are the PD control gains, and the input variables $\theta_d, \dot{\theta}_d$, and $\ddot{\theta}_d$ are the desired trajectory that the gimbaled turret is intended to follow. The output variables θ and $\dot{\theta}$ are the measured states of the system. The desired reference trajectory is found by determining the acceleration profile and then by integrating to find the velocity and position profiles. To execute a slew maneuver in the minimum amount of time, the acceleration profile is

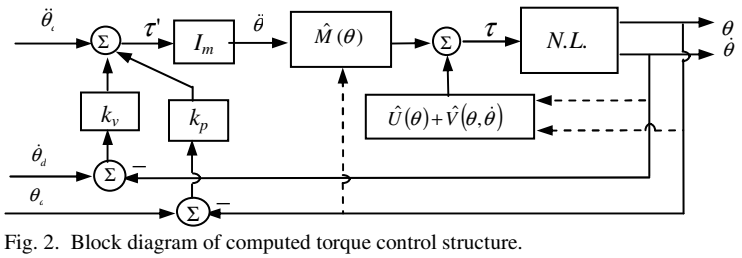

Fig. 2. Block diagram of computed torque control structure.

$$\ddot{\theta} = \begin{cases} \ddot{\theta}_{\max}, & 0 < t < \frac{1}{2}T_r \\ -\ddot{\theta}_{\max}, & \frac{1}{2}T_r < t < T_r \\ 0, & t > T_r \end{cases} \tag{7}$$

where $\ddot{\theta}_{\max}$ = the ratio of the maximum available torque to the largest effective moment of inertia resisting the torque, and

$T_r = \sqrt{\frac{4\Delta\theta}{\ddot{\theta}_{\max}}}$ is the time required to rotate a given inertia through $\Delta\theta$, given $\ddot{\theta}_{\max}$.

The velocity and position profiles are generated from this by simply performing successive integrations of (7), paying careful attention to boundary conditions. The velocity and position profiles are given by

$$\dot{\theta} = \begin{cases} \ddot{\theta}_{\max} t, & 0 < t < \frac{1}{2}T_r \\ \ddot{\theta}_{\max}(\frac{3}{2}T_r - t), & \frac{1}{2}T_r < t < T_r \\ 0, & t > T_r \end{cases}, \tag{8}$$

$$\theta = \begin{cases} \frac{1}{2}\ddot{\theta}_{\max} t^2 + \theta_0, & 0 < t < \frac{1}{2}T_r \\ \ddot{\theta}_{\max}(T_r t - \frac{1}{4}T_r^2 - \frac{1}{2}t^2) + \theta_0, & \frac{1}{2}T_r < t < T_r \\ 0, & t > T_r \end{cases}. \tag{9}$$

Figure 3 illustrates the general shape of a typical rigid-body trajectory described by these equations. For the trajectory shown in Figure 3, the turret model generated the acceleration response shown in Figure 4. Although the turret was able to achieve the steady-state angular values shown in Figure 3, the large residual acceleration of the roll shell at the end of the slew maneuver would have an adverse effect on pointing accuracy, making the early arrival of the turret at its final orientation of little benefit.

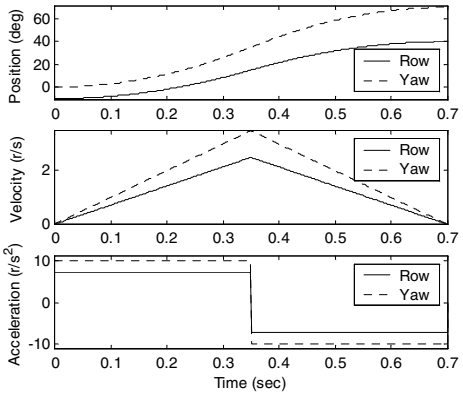

Fig. 3. Typical shape of a rigid-body trajectory.

VI. SYSTEM PERFORMANCE METRICS

The performance metric used for quantifying the amount of residual acceleration remaining at the end of a slew maneuver was defined as the root-mean-square of the roll shell acceleration over the interval, $t \in [0.86, 2.0]$ seconds.

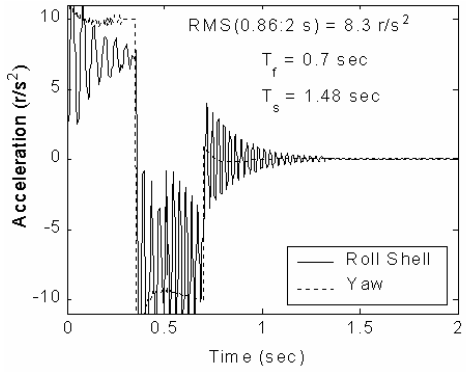

Fig. 4. Turret dynamics in response to unshaped command using gains scheduled against yaw angle.

The left boundary of the evaluation interval was selected to match the typical move times, T_f, required by the shaping methods that will be discussed next. The right-hand boundary of the evaluation interval was selected as $t = 2$ seconds to allow time for the dynamics to settle to steady state. In light of the original objective for employing the shaping techniques, that of rapid repositioning of flexible dynamic systems, perhaps the more important parameter to describe system performance is the settling time, T_s. For this investigation, T_s was defined as the time required for residual acceleration to fall within the ± 0.05 rad/sec^2 error band.

VII. INCORPORATING COMMAND SHAPING INTO FEEDBACK CONTROL

To use command shaping in conjunction with feedback control, there are a few concerns that must be addressed. The first is that the torque profile generated during the shaping process is typically not the variable around which the loop is being closed. The acceleration profile corresponding to this torque must be integrated to produce a reference trajectory that can be fed to the controller.

The second issue is that in the process of closing a feedback loop, the system resonant frequencies migrate to new locations. These are the frequencies around which the reference input must be shaped. Figure 5 illustrates the effect that closing the loop has on the system resonant frequency. The upper curve shows the variation in resonant frequency as a function of changes in the yaw angle. The lower curves show the effect of closing first the inner, and then the outer control loop.

The third consideration is that the controller must not be so overactive as to reintroduce some of the unwanted energy that the command shaping intentionally omitted. The servo-control law selected for this application was a PD controller, which might cause problems if the velocity signal was noisy or if one were required to numerically differentiate the position measurement. If finite steady state errors were a concern, one might want to use integral control to drive steady state error to zero, but this should be even more benign than derivative control, since an integrator operates primarily on the low-frequency error.

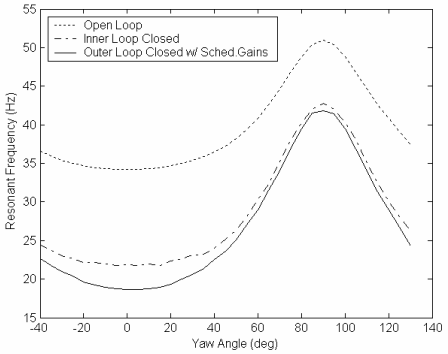

Fig. 5. Softening of roll shell drivetrain due to feedback control of turret system.

VIII. USING THE STANDARD SHAPING APPROACH

The first attempt at applying command shaping to the frequency-variant nonlinear system described by Equations (4)-(6) was to simply modify the ramped sinusoidal basis function commands, described in [6], by attenuating the magnitude of all the frequencies between the minimum and maximum values of the lowest frequency curve in Figure 5, the one corresponding to the case where both loops are closed. The resulting normalized torque profile, along with its frequency spectrum plot, is shown in Figure 6. Notice that it approximates the bang-bang torque profile, subject to the constraint imposed on the profile's spectral content.

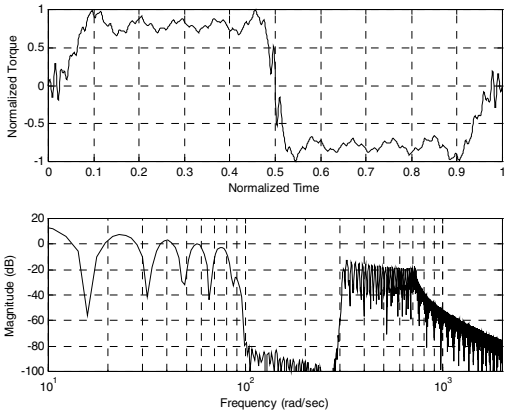

Fig. 6. Ramped sinusoidal torque profile with all frequencies from 16-45 Hz attenuated.

The acceleration associated with this torque profile was integrated to obtain the velocity profile, and then integrated again to obtain position. The resulting reference trajectory, $[\theta_d, \dot{\theta}_d, \ddot{\theta}_d]$, was then input to the closed-loop turret model, and the resulting acceleration response is shown in Figure 7. In comparing the residual acceleration of this response to

that of Figure 4, the response to this method had worse vibration, with respect to the performance metric defined in Section VI, than the case where no command shaping was attempted. Residual vibration increased by 2.4% and the settling time increased by 5.4%. One possible explanation for the dismal performance of the ramped sinusoidal approach was that the frequency notch was so wide that the controller was injecting energy into the system in the frequency range of the notch to compensate for all the missing energy.

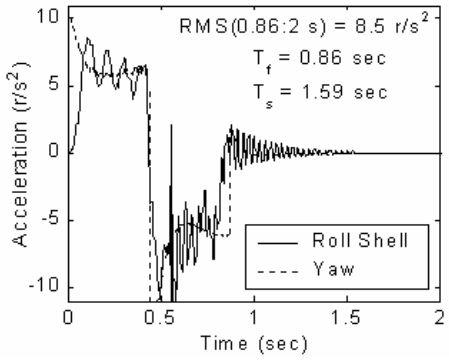

Fig. 7. Response to ramped sinusoidal shaped inputs.

IX. Possible Improvements

Command shaping using one set of ramped sinusoidal basis functions was easy to implement, and was demonstrated to be beneficial in reducing motor chatter during the slew maneuver. However, one wonders what additional improvements might be achieved by using other basis functions or more sophisticated methods of implementation, such as subdividing the slew maneuver into more than one segment and then just attenuating the energy corresponding to the resonant frequency local to that segment. One of the drawbacks of using only one set of basis functions was that the attenuated region of the shaped command's frequency response had to be large enough to cover the whole range of resonant frequencies that the nonlinear system would encounter during a given maneuver. This broad-brush approach requires the unnecessary omission of a lot of energy from the input that could otherwise be used to drive the system toward its final destination sooner. If one could somehow divide the trajectory into smaller pieces and then shape each piece separately with its own set of basis functions, then one could be more surgical in removing only the energy that would prove detrimental to the system during that segment of the move.

X. Segmented Versine Basis Function Approach

The versine basis functions were an alternative set of functions, proposed by Meckl and Seering [9], to be used in situations where one or both of the endpoint velocities were non-zero. This is exactly the situation one faces when contemplating a subdivision of the trajectory into multiple segments.

A. Generating the Versine Reference Trajectory

Having selected the versines as the new candidate basis functions, one must first perform the double integration of the versine acceleration profile to obtain the velocity and position curves. The versine torque profile is given by

$$\tau_{vs}(t) = \tau_m \sum_{k=1}^{L} \beta_k \left[1 - \cos\left(\frac{2\pi k t}{T_p} \right) \right], \tag{10}$$

where T_p is the time required to drive the system from some initial velocity to some final velocity, τ_m is the maximum available torque, and β is the coefficient-vector of the series expansion. Since there will be multiple segments, the maximum acceleration, $\ddot{\theta}_m$, was set equal to the average acceleration over each segment, i.e. to the change in velocity divided by the time length of the segment,

$$\ddot{\theta}_{vs_i}(t) = \frac{\Delta\dot{\theta}_i}{T_{p_i}} \sum_{k=1}^{L} \beta_{i,k} \left[1 - \cos\left(\frac{2\pi k t}{T_{p_i}} \right) \right]. \tag{11}$$

The maximum acceleration was thus selected to ensure that the states at the various segment boundaries match one another. Note that the coefficient-vector, β, from Equation (10) has now become a matrix, whose rows will be filled in by successive applications of the shaping algorithm, one call for each segment. The velocity profile found by integrating (11) is

$$\dot{\theta}_{vs_i}(t) = \frac{\Delta\dot{\theta}_i}{T_{p_i}} \sum_{k=1}^{L} \beta_{i,k} \left[t - \frac{T_{p_i}}{2\pi k} \sin\left(\frac{2\pi k t}{T_{p_i}} \right) \right] + \dot{\theta}_{i_o}, \tag{12}$$

and the position profile is

$$\theta_{rs}(t) = \frac{\Delta\theta_i}{T_{p_i}} \sum_{k=1}^{L} \beta_{i,k} \left[\frac{t^2}{2} + \left(\frac{T_{p_i}}{2\pi k} \right)^2 \cos\left(\frac{2\pi k t}{T_{p_i}} \right) \right] + \dot{\theta}_{i_o} t + \theta_{i_o}, \tag{13}$$

where θ_{i_o} and $\dot{\theta}_{i_o}$ are the initial position and velocity of each segment. Note that the time vector associated with each of these equations is $0 < t < T_{p_i}$. After the segment components are computed, each segment position, velocity, and acceleration is concatenated with its predecessor to form the entire trajectory.

B. Trajectory Segmentation Process

One must next decide upon the segmentation criteria. The obvious condition to impose on the size of the segments is to require that the change in the value of the resonant frequency be no larger than some pre-determined delta-frequency, Δf. The first step was to compute the rigid-body trajectory to obtain the yaw axis position profile. This profile was used to compute the closed-loop resonant frequencies of the system as a function of time. This frequency curve was then subdivided by the pre-specified Δf, and the time values corresponding to these segment boundaries were used by the next step in the process.

A less obvious requirement that should be levied on the segmentation algorithm is that segment boundaries should be aligned with discontinuities in the rigid-body torque profile arising from acceleration/deceleration transitions,

and that the average torque within a segment should be fairly representative of the actual torque over that segment. This second requirement was necessitated by the fact that the versine-shaped acceleration profile was being defined in terms of an average $\ddot{\theta}_m$ over each segment. Figure 8 shows the frequency variation in the turret model corresponding to the slew maneuver shown in Figure 3. Note that a representative set of segmentation boundaries have been superimposed on it. The number of segments for this example was six as may be observed from Figure 8.

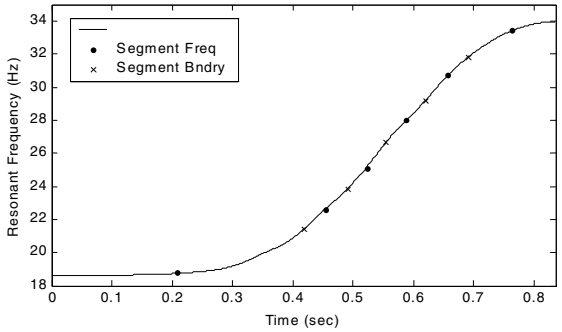

Fig. 8. Change in Resonant Frequency with Time.

Care must be taken not to overdo the number of subdivisions used, because there is a performance penalty in choosing an excessive number of segments. Every time the system reaches a segment boundary, it is constrained to momentarily achieve a zero acceleration condition, before transitioning to the next segment. Figure 9 illustrates a typical velocity profile composed of multiple segments. Note that the more segments that are required to traverse a trajectory, the greater will be the number of velocity profile inflection points through which the system must transition, thereby being hindered from reaching its final destination in the shortest possible amount of time.

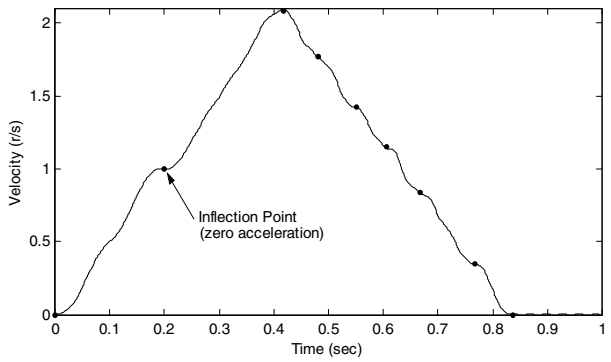

Fig. 9. Segmented velocity profile.

C. Segment Shaping Process

Following the segmentation process, the torque profiles for each of these segments was then shaped using the average resonant frequency and endpoint velocity information for each segment. From the torque profile for each segment, segment trajectories were then generated using Equations (11)-(13). This segmentation and shaping process is described in more careful detail in [8].

D. Improved Performance Using New Approach

As may be seen from Figure 10, this method was very effective in minimizing the residual vibration. When compared to the original unshaped rigid-body trajectory, this method decreased the residual roll shell acceleration by a factor of 8 and the settling time by 33%.

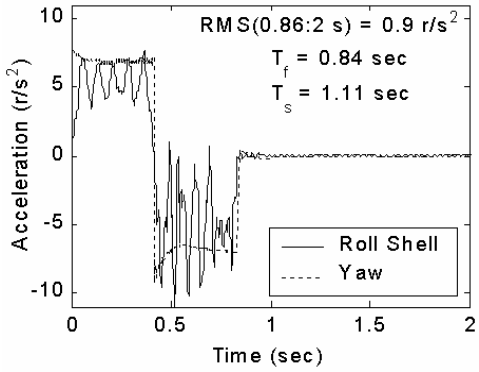

Fig. 10. Acceleration response to segmented versine -shaped inputs.

XI. Summary

A new approach to applying command shaping techniques to nonlinear systems with configuration-dependent resonant frequencies has been developed. The extension of this methodology has been illustrated to be effective in significantly reducing residual endpoint acceleration for a gimbaled telescope model that has been subjected to a large-angle slew maneuver.

References

[1]D. De Roover and F. B. Sperling, "Point-to-point Control of a High Accuracy Positioning Mechanism," *Proceedings of the American Control Conference*, Albuquerque, NM, June 1997, pp. 1350-1354.

[2]J. Park and P. H. Chang, "Learning Input Shaping Technique for Non-LTI Systems," *ASME Journal of Dynamic Systems, Measurement, and Control*, Vol. 123, June 2001, pp. 288-293.

[3]J. Park, P. H. Chang., and E. Lee, "Can a Time Invariant Input Shaping Technique Eliminate Residual Vibrations of a LTV System?" *Proceedings of the American Control Conference*, Anchorage, AK, May 2002, pp. 2292-2297.

[4]D. P. Magee, and W. J. Book, "Optimal Filtering to Minimize the Elastic Behavior in Serial Link Manipulators," *Proceedings of the American Control Conference*, Philadelphia, PA, June 1998, pp. 2637-2642.

[5]R. Kinceler, and P. H. Meckl, "Corrective Input Shaping for a Flexible-Joint Manipulator," *Proceedings of the1997 American Control Conference*, Albuquerque, NM, June 1997, pp.1335-1339.

[6]P. H. Meckl, "*Minimizing Residual Vibration of a Linear System Using Appropriately Shaped Forcing Functions*," SM Thesis, Department of Mechanical Engineering, Massachusetts Iinstitute of Technology, Cambridge, MA, June 1984.

[7]J. J. Craig, *Introduction to Robotics, Mechanics and Control*, Addison-Wesley Publishing Co, Inc., California, 1986, pp.168-172.

[8]V. M. Beazel, "*Command Shaping Applied to Nonlinear Systems with Configuration-Dependent Resonance*," Ph.D. Thesis, Dept. of Mechanical Engineering, Purdue University, West Lafayette, IN, August 2004.

[9]P. H. Meckl and W. P. Seering, "Controlling Velocity-Limited Systems to Reduce Residual Vibration," *Proceedings of 1988 IEEE Int'l Conference On Robotics and Automation*, Philadelphia, PA, April 1988, pp. 1428-1433.